

**UCLA**

**UCLA Electronic Theses and Dissertations**

**Title**

Systemic Delivery of PEGylated NEL-like Molecule-1 (NELL-1) as A Novel Strategy for Osteoinductive Therapy

**Permalink**

<https://escholarship.org/uc/item/1929n9gg>

**Author**

Park, Juyoung

**Publication Date**

2014

Peer reviewed|Thesis/dissertation

UNIVERSITY OF CALIFORNIA

Los Angeles

Systemic Delivery of PEGylated NEL-like Molecule-1 (NELL-1)  
as A Novel Strategy for Osteoinductive Therapy

A thesis submitted in partial satisfaction  
of the requirements for the degree Master of Science  
in Oral Biology

by

Juyoung Park

2014



## ABSTRACT OF THE THESIS

Systemic Delivery of PEGylated NEL-like Molecule-1 (NELL-1)  
as A Novel Strategy for Osteoinductive Therapy

by

Juyoung Park

Master of Science in Oral Biology

University of California, Los Angeles, 2014

Professor Kang Ting, Chair

NELL-1 is an osteogenic, secretory molecule previously shown to enhance bone regeneration in multiple rodent and ovine orthopedic defect models. Excitingly, we have recently shown that systemic delivery of NELL-1 induces robust bone formation in healthy and osteoporotic mice; however, like other cytokine therapies, NELL-1 has a relatively short half-life requiring a frequent dosing schedule (q2d). Here, we investigate the potential of PEGylation, a chemical process of adding polyethylene glycol (PEG), to improve NELL-1's pharmacokinetics, while maintaining bioactivity. Three different PEGylation patterns (5K-linear, 20K-linear, and 40K-branched) were covalently attached to NELL-1. First, thermostability and bioactivity of PEG-NELL-1 was compared to unmodified NELL-1 *in vitro*. Next, we evaluated the biological half-life and osteogenic potential of systemically administered PEG-NELL-1 (5K-linear, 1.25mg/kg,

i.v., q4d and q7d) in healthy mice. To monitor the changes in bone mineral density (BMD) and bone turnover rate *in vivo*, dual-energy X-ray absorptiometry (DXA) and microPET/CT bone scans was performed weekly. Animals were sacrificed after four weeks of treatment for microCT and histological analyses. PEGylation was observed to improve thermostability and biological half-life, while retaining *in vitro* bioactivity of NELL-1 protein comparable to unmodified NELL-1. *In vivo*, systemic PEG-NELL-1 therapy significantly increased femoral and lumbar BMD as well as bone turnover rate at overall skeletal sites after four weeks of treatment. MicroCT confirmed significant increases in trabecular BMD and fractional bone volume in PEG-NELL-1-treated groups. Further, immunohistochemistry revealed an increase in osteocalcin expression, while TRAP staining showed a reduction in osteoclast number in PEG-NELL-1 groups. Collectively, PEGylation significantly extends NELL-1's half-life, while retaining osteoinductive potential. Thus, PEG-NELL-1 holds promise for non-invasive, wide clinical application for the treatment of osteopenic disorders.

**Keywords:** NELL-1, PEGylation, osteoporosis, systemic osteogenic therapy

The thesis of Juyoung Park is approved.

Shen Hu

Tara Aghaloo

Kang Ting, Committee Chair

University of California, Los Angeles

2014

## TABLE OF CONTENTS

Abstract .....	ii – iii
Introduction .....	1 – 4
Current therapeutic options for osteoporosis .....	1
Identification, characterization and osteoinductive potential of NELL-1 .....	1 – 2
NELL-1’s potential as a combined anabolic/anti-osteoclastic therapeutic for osteoporosis .....	2 – 3
PEGylation technology for systemic application of NELL-1 for osteoinductive therapy .....	3 – 4
Materials and Methods .....	5 – 12
1. <i>In vitro</i> study .....	5 – 7
1.1 Thermal stability test .....	5 – 6
1.2 <i>In vitro</i> bioactivity test .....	6 – 7
1.2.1 Alkaline phosphatase (ALP) staining .....	6
1.2.2 Alizarin red s (ARS) staining .....	7
2. <i>In vivo</i> study .....	7 – 14
2.1 Biological half-life test .....	8
2.2 Systemic osteogenic potential study (at q4d and q7d injection schedules) .....	8 – 14
2.2.1 PEG-NELL-1 intravenous injection into mice .....	8 – 9
2.2.2 <i>In vivo</i> bone densitometry .....	9
2.2.3 <i>In vivo</i> microPET/CT bone scan using [ <sup>18</sup> F] fluoride ion .....	9 – 10
2.2.4 Post-mortem high-resolution microCT evaluation .....	10 – 12

## TABLE OF CONTENTS (CON'T)

2.2.5 CFU-F assay, histological and immunohistochemical analyses .....	12 – 14
3. Statistical analysis .....	14
Results .....	15 – 19
1. <i>In vitro</i> study .....	15 – 16
1.1 Thermal stability test .....	15
1.2 <i>In vitro</i> bioactivity test .....	15 – 16
2. <i>In vivo</i> study .....	16 – 19
2.1 Biological half-life test .....	16 – 17
2.2 Systemic osteogenic potential study (at q4d and q7d injection schedules) .....	17 – 19
2.2.1 <i>In vivo</i> bone densitometry .....	17 – 18
2.2.2 <i>In vivo</i> microPET/CT bone scan using [ <sup>18</sup> F] fluoride ion .....	18
2.2.3 Post-mortem high-resolution microCT evaluation .....	18 – 19
2.2.4 CFU-F assay, histological and immunohistochemical analyses .....	19
Discussion .....	20 – 22
Conclusion .....	23
Figures and Tables .....	24 – 36
References .....	37 – 39

## LIST OF FIGURES AND TABLES

Figure 1: Structure and function of NELL-1 .....	24
Figure 2: Schematic diagram of PEG-NELL-1 synthesis .....	25
Figure 3: Thermal shift assay result of NELL-1 and PEG-NELL-1 (5K, 20K, 40K) measured by thermofluor method .....	26
Figure 4: Effects of PEGylation on pro-osteogenic bioactivity of NELL-1 protein <i>in vitro</i> .....	27
Figure 5: Effects of PEGylation on biological half-life of NELL-1 protein .....	28
Figure 6: Dual-energy X-ray absorptiometry (DXA) taken weekly to monitor the changing BMD .....	29 – 30
Figure 7: MicroPET/CT bone scan using [ <sup>18</sup> F] fluoride ion to assess bone turnover rate over the skeleton .....	31
Figure 8: Post-mortem microCT results at 4 weeks post-treatment .....	32 – 33
Figure 9: CFU-F assay results from PEG-NELL-1 (q7d) and PEG/PBS control groups at 4 weeks post-treatment .....	34
Figure 10: Histological and immunohistochemical staining results .....	35
Table 1: Summary of PEGylated NELL-1 types .....	36

## ACKNOWLEDGMENTS

Chapter 1 and Chapter 2.1 of this study is a version of the work published in *Biomaterials* 2014; 35(24): 6614-6621, on which the copyright is reserved by Elsevier. The title and co-authors of the published material are as follows:

### **Bioactivity and circulation time of PEGylated NELL-1 in mice and the potential for osteoporosis therapy**

Yulong Zhang <sup>a, b</sup>, Omar Velasco <sup>c</sup>, Xinli Zhang <sup>c</sup>, Kang Ting <sup>c, d</sup>, Chia Soo <sup>c, d</sup>, Benjamin M. Wu  
a, b, c, d, \*

\* Corresponding author

<sup>a</sup> Department of Bioengineering, <sup>b</sup> Department of Materials Science and Engineering, and Division of Advanced Prosthodontics, <sup>c</sup> Weintraub Center for Reconstructive Biotechnology, and Dental and Craniofacial Research Institute, School of Dentistry, <sup>d</sup> Department of Orthopaedic Surgery, University of California, Los Angeles, Los Angeles, CA 90095, USA.

The author thanks Yulong Zhang for kindly granting permission to reuse his works. This work was supported by the CIRM Early Translational II Research Award TR2-01821, NIAMS R01 AR066782-01, NIAMS R01 AR061399-01A1, and Eli & Edythe Broad Center of Regenerative Medicine and Stem Cell Research at UCLA Innovation Award. Drs. X.Z., K.T., and C.S. are inventors of Nell-1 related patents. Drs. X.Z., K.T., and C.S. are founders and/or board members of Bone Biologics Inc. which sublicenses Nell-1 patents from the UC Regents, which also hold equity in the company.

## INTRODUCTION

### *Current therapeutic options for osteoporosis*

Osteoporosis, the most common metabolic bone disease, affects over 200 million people worldwide with 10 million people affected in the United States alone (Berry et al., 2010; Czerwinski et al., 2007; Heinemann, 2000; Jilka, 2003; Shuler et al., 2012; Watts et al., 2008). Therapeutic approaches to osteoporotic bone loss have focused thus far on either anabolic or antiresorptive agents (Bilezikian, 2008; Cusano and Bilezikian, 2012) with only one anabolic agent, parathyroid hormone (PTH), FDA-approved for the temporary treatment of osteoporosis. To address the pressing need for new therapies that are both anabolic and anti-osteoclastic (Cusano and Bilezikian, 2012; Jilka, 2007; Neer et al., 2001; Vahle et al., 2002), new agents that increase Wnt/ $\beta$ -catenin activity have been developed. Wnt/ $\beta$ -catenin signaling plays a key role in directing stem cell differentiation to osteoblasts (OB) and inhibiting osteoclast (OC) activity (Minear et al., 2010; Wagner et al., 2011). In addition, decreased Wnt/ $\beta$ -catenin signaling has been implicated in osteoporosis (Cabrera et al., 1987; Nusslein-Volhard and Wieschaus, 1980). However, as recombinant Wnts are difficult to produce and deliver, most approaches to increase Wnt/ $\beta$ -catenin signaling block naturally occurring Wnt antagonists via antibodies (e.g., anti-DKK1 or anti-Sclerostin antibodies) (Minear et al., 2010; Wagner et al., 2011) to functionally ‘de-repress’ Wnt signaling.

### *Identification, characterization and osteoinductive potential of NELL-1*

NELL-1 (NEL-like molecule-1), a unique secretory molecule, was first implicated in bone formation by its overexpression in human craniosynostosis (Ting et al., 1999). Specifically, NELL-1 is a 700 kDa protein recognized as a potent pro-osteogenic cytokine (**Figure 1A**), and

was most often studied for its local bone forming effects in various small and large animal models (Aghaloo et al., 2006; Aghaloo et al., 2007; Cowan et al., 2012; James AW, 2013; Kwak et al., 2013; Li et al., 2010; Lu et al., 2007; Siu et al., 2011). For example, NELL-1 was reported to induce robust osseous healing of critical-sized rat femoral segmental and calvarial defects (Li et al., 2011; Aghaloo et al., 2006; Aghaloo et al., 2010; Zhang et al., 2011), and also to promote lumbar spinal fusion in rats, sheep (Li et al., 2010; Lu et al., 2007; Siu et al., 2011) and non-human primates. Additionally, NELL-1 has recently been identified to have anti-osteoclastic effects both *in vitro* and *in vivo* (James AW, 2013) and to suppress adipogenesis (James et al., 2011) (**Figure 1B**).

#### *NELL-1's potential as a combined anabolic/anti-osteoclastic therapeutic for osteoporosis*

Recently, an association between NELL-1 and osteoporosis was described, where a genome-wide linkage study identified *NELL-1* polymorphisms in patients with reduced BMD (Karasik et al., 2010). In accordance with this, our preliminary studies indicated that, like Wnt/ $\beta$ -catenin, NELL-1 can act as a combined anabolic and anti-osteoclastic agent to protect against osteoporotic bone loss. Not only are *Nell-1* haploinsufficient mice more prone to osteoporosis, but local delivery of NELL-1 also reverses osteoporotic bone loss in both small and large animal models (Kwak et al., 2013). Excitingly, we have recently determined that NELL-1 effects occur in large part via activation of Wnt/ $\beta$ -catenin signaling (James AW, 2013) and also that systemically delivered NELL-1 potently reverses ovariectomy (OVX)-induced bone loss in mice, but with a relatively frequent administration (q2d; 3-4 doses/week) (Asatrian et al., 2013) due to the rapid clearance of the native protein. The short circulation time of NELL-1 *in vivo* was deemed as one of the main limitations for its practical application in a systemic therapy.

Therefore, the main purpose of the present study was to modify the structure of NELL-1 and improve its pharmacokinetics to extend its circulation time *in vivo*.

#### *PEGylation technology for systemic application of NELL-1 for osteoinductive therapy*

For the past decade, various technologies have been developed to achieve desirable pharmacokinetic properties of therapeutic proteins. These technologies include amino acid engineering, genetic fusion to immunoglobulin domains or serum proteins, and conjugation with natural or synthetic polymers (polysialylation, HESylation, and PEGylation), among which PEGylation is the most established, widely used, FDA-approved technology to prolong biological half-life of a protein (Jevsevar et al., 2010). PEGylation is a chemical process of covalently attaching water-soluble polyethylene glycol (PEG) polymers to a target molecule in order to modify the molecule's physiologic and pharmacokinetic characteristics. (Jevsevar et al., 2010; Levy et al., 1988; Ng et al., 2006). PEGylation can be achieved by incubating a reactive PEG derivative with the target molecule. For instance, chemically activated PEG-N-hydroxysuccinimide (PEG-NHS) is highly reactive with amine group in lysine residue of a target protein at a physiological pH (Nojima et al., 2009). Through PEGylation, the hydrodynamic size of a therapeutic protein increases, resulting in reduced renal clearance and extended half-life. In addition, adding PEG can protect the target protein from the host immune system and improve the safety of the agent (Jevsevar et al., 2010). Thus far, the Food and Drug Administration (FDA) has approved 9 marketed PEGylated therapies.

In this study, we hypothesize that PEGylation of NELL-1 is an effective approach to develop NELL-1 into a systemic therapeutic. To test this, we aim to conduct the study in two folds - *in*

*vitro* and *in vivo*. *In vitro*, we will test three types of PEGylation patterns to examine their effects on the NELL-1 protein in regards to thermostability and bioactivity. *In vivo*, we will first test the different PEGylation types for biological half-life. Then, based on the *in vitro* tests and *in vivo* half-life result, we will select the optimal type of PEGylation for the subsequent *in vivo* study, where we will examine the osteogenic potential of systemically administered PEGylated NELL-1 (PEG-NELL-1) compared to carrier control. Considering that the systemic anti-osteoporosis therapeutics currently in development (e.g., anti-DKK1, anti-Sclerostin antibodies) are given q4d (2 doses/week) (Glantschnig et al., 2011), we sought to examine the osteogenic potential of PEG-NELL-1 administered at q4d and q7d. An injection frequency reduced to q7d (one dose/week) would be the first step toward the development of NELL-1 into systemic therapeutics to treat osteopenic disorders, with better patient compliance in chronic treatment clinical settings.

## MATERIALS AND METHODS

### *1. In vitro study*

First, to assess the effect of PEGylation on NELL-1's stability and osteogenic potential, three PEGylation patterns (5K-linear, 20K-linear, and 40K-branched) were evaluated for 1) thermostability and 2) pro-osteoblastic bioactivity *in vitro* on mouse calvarial osteoblast cells and human adipose-derived perivascular stem cells (hPSC).

PEGylated NELL-1 (PEG-NELL-1) was synthesized from linear PEG-NHS Mw=5kDa (Sigma-Aldrich, MO), linear PEG-NHS Mw=20kDa (NOF America corporation, Japan), and 4-arm-branched PEG-NHS Mw=40kDa (NOF America corporation, Japan) according to the PEGylation protocol similar to those described by Bansal et al. (Bansal et al., 2011). Briefly, PEGylation of NELL-1 was attained by a reaction in which the N-hydroxysuccinimide group of PEG-NHS was covalently linked to the  $\epsilon$ -amine group on lysine side chains or the  $\alpha$ -amine group of NELL-1 protein (**Figure 2**). Obtained PEG-NELL-1 was then purified using a Sephadex G-25M column (Sigma-Aldrich, MO), and dialyzed using dialysis cassettes (Fisher Scientific, Inc., MA) to remove unreacted PEG molecules. The schematic structure and PEG modification degree of each PEG-NELL-1 type measured by fluorometric assay using fluorescamine are presented in **Table 1**.

#### *1.1 Thermal stability test*

The thermal stability of PEG-NELL-1 was evaluated by thermal shift assay method using a 7300 real-time PCR system (Applied Biosystems, CA). Prior to using, fluorescent SYPRO Orange stock solution in DMSO (5000x, Sigma-Aldrich, MO) was diluted 1:125 in phosphate

buffered saline (PBS). The samples were prepared in a 96-well plate in triplicate containing 3  $\mu$ l of PEG-NELL-1 (1 mg/ml), 2.5  $\mu$ l of freshly diluted SYPRO Orange (40x) and 19.5  $\mu$ l of PBS buffer (0.01M, pH 7.4), then the plate was sealed with optical quality sealing tape and centrifuged at 4000 rpm for 2 min. The fluorescent intensity was monitored as the plate was heated from 298 to 368k in increments of 1 K/min, and was analyzed using a Boltzmann model, from which the melting point ( $T_m$ ) was calculated.

## *1.2 In vitro bioactivity test*

### *1.2.1 Alkaline phosphatase (ALP) staining*

The bioactivity of PEG-NELL-1 was assessed in two aspects: early and terminal osteoblast differentiation. To assess early differentiation of osteoblasts, the expression of alkaline phosphatase (ALP) was examined in mouse calvarial osteoblast cells isolated from frontal and parietal bones of 3-5 days old C57BL/6 mice. Extracted cells were expanded in Dulbecco's modified Eagle's medium (DMEM) containing 10% fetal bovine serum (FBS) at 37°C and 5% CO<sub>2</sub>, and passage 2 cells were used for the experiment. For ALP staining, the cells were cultured for 9 days in an osteogenic medium supplemented with 3 different types of PEG-NELL-1 (300 ng/ml), unmodified NELL-1 (300 ng/ml) or control PBS to induce osteoblastic differentiation, then lysed using lysis buffer (0.2% NP-40 and 1 mM magnesium chloride). The cell lysate was mixed with ALP substrate buffer (0.4 mg p-nitrophenyl phosphate, 0.1 ml alkaline buffer A, and 0.1 ml distilled water), and the relative staining intensity was measured at 405 nm and normalized to the amount of protein in the corresponding well. The measurements were performed in triplicate for each sample.

### 1.2.2 Alizarin red s (ARS) staining

To assess terminal differentiation of osteoblasts and bone nodule formation, calcium phosphate mineralization was assessed using alizarin red s (ARS) staining in hPSCs isolated from fresh adipose tissues as previously described (James et al., 2012). Extracted cells were expanded in DMEM containing 20% FBS at 37°C and 5% CO<sub>2</sub>, and passage 2 cells were used for the experiment. For ARS staining, the hPSCs were cultured for 15 days in an osteogenic medium supplemented with 3 different types of PEG-NELL-1 (300 ng/ml), unmodified NELL-1 (300 ng/ml) or control PBS to induce osteoblastic differentiation, then fixed with 10% formaldehyde for 15 min. The fixed cells were washed and stained with ARS solution (40 mM, pH 4.2) for 20 min, and the wells containing stained mineralized nodules were imaged by digital camera. Then, alizarin red stain was leached from cells in 10% acetic acid by heating to 85°C for 10 min. The cell lysate was centrifuged and the supernatant was quantified at 450 nm. The experimental conditions were performed in quadruplicate.

### 2. *In vivo* study

Next, to examine the effect of PEGylation *in vivo*, 3-month old female CD-1 mice (n=24, mean body weight 20g, Charles River Laboratories, MA) were used for biological half-life study and 3-month old female C57BL/6 mice (n=22, mean body weight 20g, Jackson Laboratory, ME) were used for systemic osteogenic potential study, respectively. Animals were housed in a light- and temperature-controlled environment and given food and water *ad libitum*. All animals were handled in accordance with institutional guidelines of the Chancellor's Animal Research Committee (ARC) of the Office for Protection of Research Subjects at the University of California, Los Angeles.

## *2.1 Biological half-life test*

To test the effect of PEGylation on systemic circulation time, fluorescein isothiocyanate (FITC)-labeled NELL-1 and PEG-NELL-1 (5K, 20K, and 40K) were used. Briefly, 50 µg of FITC (Sigma-Aldrich, MO) was added to 0.25 ml of NELL-1 or PEG-NELL-1 (4 mg/ml) in a 0.1 M sodium carbonate-bicarbonate buffer (pH 9.0), and reacted for 3 hours at room temperature. The FITC-labeled NELL-1 and PEG-NELL-1 were purified from unreacted FITC using a Sephadex G-25M column (Sigma-Aldrich, MO), and stored in light-protected (foil-wrapped) vials at -20°C before use. Next, 24 CD-1 mice were randomly assigned to 4 groups (n=6/group) and injected with a 100 µl single dose of FITC-labeled proteins (1.25 mg/kg) via the lateral tail veins. Blood samples were collected from retro-orbital sinus at 0.5 and 24 hours after injection, transferred into the serum separator tube, and the serum was separated by centrifugation at 10,000 rpm for 5 min. The concentrations of unmodified NELL-1 and PEG-NELL-1 in serum were analyzed by the fluorescence intensity of FITC using a plate reader (Infinite F200, Tecan Group Ltd., Switzerland).

## *2.2 Systemic osteogenic potential study (at q4d and q7d injection schedules)*

### *2.2.1 PEG-NELL-1 intravenous injection into mice*

To investigate the osteogenic capacity of systemically administered PEG-NELL-1, 22 C57BL/6 mice were randomly divided into 4 groups: PEG/PBS control (q4d, n=3), PEG/PBS control (q7d, n=3), PEG-NELL-1 (q4d, n=8), and PEG-NELL-1 (q7d, n=8). Then, the mice were intravenously injected with a 100 µl dose of PEG/PBS or PEG-NELL-1 via the lateral tail veins at q4d or q7d dosing interval over the 4-week experimental period. The optimal doses for PEG/PBS (1.52 mg/kg) and PEG-NELL-1 (1.25 mg/kg) were determined according to our

previous study (Asatrian et al., 2013), and NELL-1 PEGylated with 5kDa PEG (PEG-NELL-1 (5K)) was chosen based on the *in vitro* and the *in vivo* half-life results from this study. All animals were anesthetized with isoflurane during the procedure. Animals were warmed to dilate the veins by soaking the tails in warm water for 5-10 minutes prior to injection. After injection, animals were monitored to ensure hemostasis.

### 2.2.2 *In vivo bone densitometry*

To monitor bone mineral density (BMD), dual-energy X-ray absorptiometry (DXA) scan was performed weekly using a Lunar PIXImus II Densitometer (GE Lunar, WI). Under isoflurane anesthesia, all animals were positioned prone on the imaging pad with the femurs parallel to scan direction and knee joints flexed at a right angle. Areal BMD was determined with rectangular regions-of-interest (ROIs) placed on distal femur and lumbar vertebrae (L6) using image analysis software (version 2.10) provided by the manufacturer. Data at each time point were generated as relative percent changes in BMD compared to respective pre-treatment values at week 0 (**Figure 6**).

### 2.2.3 *In vivo microPET/CT bone scan using [<sup>18</sup>F] fluoride ion*

To monitor the overall bone metabolic activity, [<sup>18</sup>F] fluoride ion bone scanning was performed weekly using micro positron emission tomography (microPET) and correlated with anatomical imaging using micro computed tomography (microCT) at the UCLA Crump Institute for Molecular Imaging. In brief, [<sup>18</sup>F] fluoride ion was produced at specific activities of approximately 1,000 Ci/mmol using <sup>18</sup>O-labeled water and proton bombardment using a RDS cyclotron (Siemens Medical Solutions USA, Inc., TN). Mice were injected with [<sup>18</sup>F] fluoride

ion (less than 200  $\mu\text{Ci}$ ) via lateral tail veins and kept anesthetized with isoflurane during radioactive probe uptake and clearance for 1 hour, followed by microPET (FOCUS 220 system; Siemens Medical Solutions USA, Inc., TN) and microCT (microCAT II; Siemens Medical Solutions USA, Inc., TN) combination scans lasting 20 min. All animals were imaged within ARC-approved rodent imaging chambers to minimize positioning errors during co-registration between microPET and microCT images. MicroPET images were reconstructed using filtered back projection (FBP) and an iterative three-dimensional *maximum a posteriori* (MAP) reconstruction algorithm, and co-registered with the microCT images to ensure proper anatomical location of ROIs. Then, images were analyzed and quantified using AMIDE (A Medical Image Data Examiner) software (version 1.0.4). Mean tissue activity concentration ( $\mu\text{Ci}/\text{ml}$ ) of [ $^{18}\text{F}$ ] fluoride ion was determined by cylindrical ROIs drawn on distal femur and lumbar vertebrae, and normalized to the injected dose ( $\mu\text{Ci}$ ). Data at each time point were expressed as the percent of decay-corrected injected activity per milliliter of tissue, using the formula shown in **Figure 7**.

#### 2.2.4 Post-mortem high-resolution microCT evaluation

Animals were sacrificed at 4 weeks post-treatment and harvested for left and right femurs, tibias, humeri, and thoracic and lumbar vertebrae. Fluorochrome-labeled samples were fixed and stored in 70% ethanol (EtOH), and the remaining samples were fixed in 4% paraformaldehyde (PFA) for 48 hours and stored in 70% EtOH for microCT, histological and immunohistochemical analyses. Postharvest, femurs and lumbar vertebrae were scanned using a high-resolution microCT (SkyScan 1172; SkyScan N.V., Belgium) at image resolutions of 27.4  $\mu\text{m}$  and 7.95  $\mu\text{m}$  (55kV and 181 mA radiation source, using a 0.5-mm aluminum filter). Then, 3D images were

reconstructed from the 2D X-ray projections by implementing the Feldkamp algorithm, and appropriate image corrections including ring artifact correction, beam hardening correction and fine-tuning were processed using NRecon software (SkyScan N.V., Belgium). The dynamic image range (contrast limits) was determined at 0-0.1 in units of attenuation coefficient and applied to all datasets for optimum image contrast.

After acquisition and reconstruction of datasets, images were first viewed and reoriented on each 3D plane using DataViewer software (SkyScan N.V., Belgium) to align the long axes of femur and vertebral body parallel to coronal and sagittal planes. Then, 3D morphometric analysis of the distal femur and the body of lumbar vertebrae was performed using CT-Analyzer software (SkyScan N.V., Belgium). For femurs, the most proximal point of the growth plate and the proximal end of the third trochanter were set as reference levels along the long axis from which to divide the femurs into ten segments of equal thickness (1 mm = 36 slices). The trabecular region was defined as the first three distal segments to include secondary spongiosa in the distal metaphysis. Within the trabecular region, ROIs were delineated every 5-10 transaxial slices using a freehand drawing tool to separate trabecular structures from endocortical bone by maintaining 3.5-pixel clearance from the endosteal surface. In lumbar vertebrae, a full vertebral body length excluding growth plate regions near articular surfaces was selected as the trabecular region within which ROIs were drawn using the same manual contouring method as in femurs. ROI shapes were automatically morphed between edited slices.

A global threshold of 60 ( $1.01573 \text{ g/cm}^3$ ) was applied to all scans to extract physiologically accurate representation of trabecular bone phase. Morphometric parameters were then computed

from the binarized images using direct 3D techniques (Marching cubes and sphere-fitting methods), and included bone mineral density (BMD,  $\text{g}/\text{cm}^3$ ), bone volume fraction (BV/TV, %), trabecular number (Tb.N,  $\text{mm}^{-1}$ ), trabecular thickness (Tb.Th, mm) and trabecular separation (Tb.Sp, mm). All quantitative and structural parameters followed the nomenclature and units recommended by the American Society for Bone and Mineral Research (ASBMR) Histomorphometry Nomenclature Committee (Parffit et al., 1987). After data quantification, 3D rendered models were generated for the visualization of analyzed regions using the Marching cubes method.

#### *2.2.5 CFU-F assay, histology and immunohistochemical analyses*

For the colony-forming unit-fibroblast (CFU-F) assay, freshly harvested left and right humeri were used to isolate bone marrow stem cells (BMSCs) by marrow flushing. Isolated marrow cells were seeded on 6-well plates ( $1 \times 10^6$  cells/well), and cultured for 10 days in Complete MesenCult Medium (STEMCELL Technologies, Inc., Canada) at  $37^\circ\text{C}$  in 5%  $\text{CO}_2$ . CFU-F-derived colonies were stained using Giemsa Staining Solution (EMD Chemicals, Inc., NJ) for 5 minutes, and were counted microscopically.

After microCT scans, the samples were decalcified using 19% EDTA solution for 14 days, dehydrated, and processed for paraffin embedding. Five- $\mu\text{m}$  thickness longitudinal sections were cut on a microtome, and the slides were either stained with hematoxylin and eosin (H&E) or with markers of osteoblast (osteocalcin: OCN) and osteoclast (tartrate-resistant acid phosphatase: TRAP) as previously described (Shen et al., 2013).

For immunohistochemical staining, slides were deparaffinized, rehydrated, and incubated with 3% H<sub>2</sub>O<sub>2</sub> for 20 minutes, and blocked with 0.1% bovine serum albumin (BSA) in PBS for 1 hour. Primary antibody to OCN (Santa Cruz Biotechnology, Inc., TX) at a 1:100 dilution was applied to each section and incubated at 37°C for 1 hour and then at 4°C overnight. Biotinylated secondary antibody (Dako, Inc., CA) at a dilution of 1:200 was added and incubated for 1 hour at room temperature, followed by detection with the ABC avidin-peroxidase enzyme complex (Vectastatin Elite ABC Kit; Vector Laboratories, Inc., CA) and the AEC chromogenic substrate (Dako, Inc., CA). Then, sections were counterstained with hematoxylin. PBS substituted for the primary antibody was used as a negative control.

For TRAP staining, an Acid Phosphatase, Leukocyte (TRAP) Kit (Sigma-Aldrich, MO) was used according to the manufacturer's protocol. Briefly, sections were immersed in TRAP staining solution (12.5 mg/ml Naphthol AS-BI phosphoric acid, 2.5 M acetate buffer, diazotized Fast Garnet GBC solution, and deionized water) at 37°C for 60 min, protected from light. Subsequently, sections were rinsed thoroughly in deionized water and counterstained with hematoxylin.

Histological and immunohistochemical specimens were analyzed using an Olympus BX51 microscope (Olympus Corporation, Japan) and photomicrographs were acquired using a MicroFire digital camera with PictureFrame software (Optronics, CA). OCN and TRAP staining were analyzed by three blinded observers, and quantified by the number of osteoblasts per trabecular bone perimeter (N.Ob/B.Pm, mm<sup>-1</sup>) and the number of osteoclasts per trabecular bone

perimeter (N.Oc/B.Pm,  $\text{mm}^{-1}$ ) respectively. The reported results were the average of data obtained from six random fields per sample.

### *3. Statistical analysis*

Means and standard deviations were calculated from numerical data. Statistical analyses were performed using one-way analysis of variance (ANOVA) test for multiple comparisons and Student's t-test for two-group comparisons at 95% confidence levels. Data are presented as mean  $\pm$  SD, with \* $P < 0.05$  and \*\* $P < 0.01$ .

## RESULTS

### *1. In vitro study*

#### *1.1 Thermal stability test*

The thermal stability of the PEG-NELL-1 was examined by thermal shift assay. The fluorescent curves of NELL-1 and PEG-NELL-1 (5K, 20K, and 40K) are shown in **Figure 3A**, and the  $T_m$  of corresponding proteins analyzed by Boltzmann model is shown in **Figure 3B**. The  $T_m$  of NELL-1 was 49.75°C, but after PEGylation, the  $T_m$  increased up to 63.42°C (27% increase in PEG-NELL-1 (5K)). The protein unfolding curves of NELL-1 shifted to higher temperature after PEGylation, suggestive of enhanced stability of the protein. Interestingly, the thermal stability of PEG-NELL-1 (5K) was much higher than that of PEG-NELL-1 with higher PEG molecular weight (20K and 40K), suggesting that the more PEG molecules linked to a NELL-1 protein, the higher the stabilizing effect. In fact, fluorometric assay to evaluate PEG modification degree showed that a PEG-NELL-1 (5K) contains 31.5 PEG molecules while PEG-NELL-1 (20K) and PEG-NELL-1 (40K) contain only 20.4 and 6.2 PEG molecules respectively.

#### *1.2 In vitro bioactivity test*

The bioactivity of PEG-NELL-1 assessed in mouse calvarial osteoblasts and human PSCs showed a similar trend in *in vitro* osteogenic capacity (**Figure 4**). All three PEGylation patterns not only promoted osteoblastic differentiation of mouse calvarial cells as shown in ALP staining, but also increased hPSC mineralization as indicated by ARS staining. Although all types of PEG-NELL-1 showed slightly decreased bioactivity compared to unmodified NELL-1 (non-significant), they all showed significantly increased bioactivity compared to the negative control

(PBS). The reduced bioactivity of PEG-NELL-1 compared to NELL-1 can be attributed to the weakened interaction between the cell and NELL-1 protein which is masked by PEG molecules. These results suggest that although PEGylation affects the bioactivity of NELL-1, PEG-NELL-1 still effectively enhances the osteogenic potential of the cells. The representative plates and quantified relative bioactivity of PEG-NELL-1 determined by ARS assay of hPSCs are also shown in **Table 1**.

## *2. In vivo study*

### *2.1 Biological half-life test*

To assess the effect of PEGylation on NELL-1's pharmacokinetics, a single bolus of FITC-labeled NELL-1 or PEG-NELL-1 was injected into mice and blood samples were collected at two different time points (0.5 and 24 hours) to monitor protein concentrations in blood. The remaining amount (%ID: percent injected dose) of the protein was measured by the fluorescence intensity of FITC. At 0.5 hours after injection, only 9.3% of the initial dose remained in the blood samples of mice injected with unmodified NELL-1, while significantly higher amounts of circulating protein (%ID=22.6 for PEG-NELL-1 (5K), 67.1 for PEG-NELL-1 (20K), and 44.0 for PEG-NELL-1 (40K)) were detected with PEG-NELL-1 administration (**Figure 5**). After 24 hours from injection, all types of PEG-NELL-1 still maintained considerably higher blood concentrations compared to that of unmodified NELL-1 with which only an infinitesimal amount was left in blood (**Figure 5**). Among PEG-NELL-1 types examined, PEG-NELL-1 (20K) exhibited the highest blood concentrations at 0.5 and 24 hours, which corresponds to a higher molecular weight and larger hydrodynamic size of PEG-NELL-1 (20K) than other types of PEG-NELL-1 (5K and 40K). Calculated elimination half-life of NELL-1 and each type of PEG-

NELL-1 are presented in **Table 1**. Collectively, PEGylation successfully prolonged the circulatory time of NELL-1 from 5.5 hours to 14.5-31.3 hours (up to 6-fold) *in vivo*, enabling reduced injection frequency. Based on the results from *in vitro* thermostability and bioactivity tests and *in vivo* half-life test, PEG-NELL-1 (5K) was selected for the subsequent systemic osteogenic potential study.

## *2.2 Systemic osteogenic potential study (at q4d and q7d injection schedules)*

### *2.2.1 In vivo bone densitometry*

To monitor the changing BMD in the femurs and lumbar vertebrae of systemically treated mice, DXA was performed weekly. Results were expressed as percent changes in areal BMD relative to the respective pre-treatment values at week 0. For PEG/PBS control groups, BMD remained steady at baseline levels in both distal femur and lumbar vertebrae (L6) for the experimental period. Contrariwise, distal femurs in both q4d and q7d PEG-NELL-1 groups showed gradual and significant increases in BMD (16% and 11% respectively) by 4 weeks post-treatment, compared to pre-treatment values. Both q4d and q7d PEG-NELL-1 femurs demonstrated significantly greater BMD values compared to the cognate vehicle controls, but with no significant difference between each other at week 4 (**Figure 6A**). Similarly, lumbar vertebrae in both PEG-NELL-1 groups exhibited increasing BMD relative to the baseline throughout the experiment, with more BMD increment observed in q7d PEG-NELL-1 group (11%) than in q4d PEG-NELL-1 group (4%) at week 4. Although only a moderate lumbar BMD increase was found with q4d PEG-NELL-1 group compared to the control, q7d PEG-NELL-1 lumbar vertebrae showed significantly higher BMD increase than that of the vehicle-treated

group after 4 weeks of treatment. No significant difference in lumbar BMD was observed between the two experimental groups at week 4 (**Figure 6B**).

### 2.2.2 *In vivo microPET/CT bone scan using [<sup>18</sup>F] fluoride ion*

Next, the physiological bone turnover over the mouse skeleton was examined by weekly microPET/CT combination scan using [<sup>18</sup>F] fluoride ion. Live-microCT revealed increased bone mineral density in PEG-NELL-1 (q7d) group at the overall skeletal sites, compared to control mice (**Figure 7A**). [<sup>18</sup>F] fluoride ion is substituted for hydroxyl groups in hydroxyapatite and covalently bonds to the surface of new bone. Thus, uptake is higher in newly formed bone (osteoid) due to higher availability of binding sites. MicroPET revealed increased bone turnover rate in PEG-NELL-1 (q7d) group with higher activity distribution particularly near growth plate areas in the vertebral column, proximal humeri, proximal and distal femurs, and proximal tibias (**Figure 7B**). These hot spots were then selected for the sites of analysis by post-mortem microCT.

### 2.2.3 *Post-mortem high-resolution microCT evaluation*

In line with the *in vivo* DXA and microPET bone scan results, post-mortem microCT confirmed considerable improvement in the trabecular bone density (BMD), bone volume fraction (BV/TV), and structural parameters (Tb.Th, Tb.N, Tb.Sp) in femurs of both q4d and q7d PEG-NELL-1 groups at 4 weeks post-treatment, compared to corresponding PEG/PBS control (**Figure 8A-E**). Both PEG-NELL-1 groups demonstrated statistically significant increase in bone volume fraction (BV/TV) compared to the control, but with no substantial difference between each other (**Figure 8B**). The q7d PEG-NELL-1 group showed significant improvement in all the

other trabecular parameters as well (BMD, Tb.Th, Tb.N, and Tb.Sp) compared to the control (**Figure 8A-E**).

#### *2.2.4 CFU-F assay, histological and immunohistochemical analyses*

To examine bone marrow mesenchymal stem cell (BMSC) content, CFU-F assay was performed using fresh and passaged bone marrow isolates from humeri immediately post-harvest. The results at 4 weeks post-treatment showed a statistically significant increase of BMSC number in PEG-NELL-1 (q7d) group compared to control, suggesting that PEG-NELL-1 enhances the proliferation of BMSCs when administered systemically (**Figure 9**). The H&E stain confirmed increased bone formation and trabeculation in the metaphyseal area of distal femur in PEG-NELL-1 treatment group. Consistently, OCN immunostaining demonstrated increased osteoblast number while TRAP staining showed decreased osteoclast number in the PEG-NELL-1-treated group compared to PEG/PBS control group (**Figure 10**).

## DISCUSSION

Osteoporosis, characterized by decreased bone mass and deterioration of bone microarchitecture, is a common metabolic bone disease with associated bone fragility and increased risk of fracture. As bone loss in osteoporosis occurs insidiously, it is often diagnosed after the first clinical fracture has occurred. Therefore, the aim of therapy is usually prevention of further fractures. Therapeutic approaches to osteoporotic bone loss have focused on either antiresorptive or anabolic agents. Antiresorptive agents such as bisphosphonates slow down bone resorption. Specifically, denosumab is an antibody to receptor activator of nuclear factor kappa-B ligand (RANKL) that inhibits osteoclast differentiation and function, and odanacatib is a drug in phase III development which inhibits cathepsin K (CTSK), a protease secreted by osteoclast to degrade collagen matrix. On the other arm, anabolic agents stimulate bone formation. Thus far, only one anabolic agent, parathyroid hormone (PTH) is FDA approved for treatment of osteoporosis. Although present therapies are efficient, there has been a pressing need to develop new agents due to poor long-term adherence and considerable adverse effects related to currently available therapeutics.

A drug targeting Wnt signaling is unique in that it has dual anabolic and anti-resorptive functions with potential in reversing osteoporosis. This is obvious when we consider the role of Wnt signaling with respect to bone metabolism. Wnt signaling favors mesenchymal stem cell fate toward osteogenic differentiation by directly activating Wnt targeted osteogenic genes. On the other hand, Wnt inhibits adipogenic differentiation through regulating the expression of the master adipogenic factor, peroxisome proliferator-activated receptor gamma (PPAR $\gamma$ ) (Takada et al., 2009). In addition, Wnt can inhibit osteoclastogenesis either by directly regulating osteoclast

or indirectly by inducing osteoprotegerin (OPG) production by osteoblast (Albers et al., 2013). Therefore, manipulating the Wnt pathway may offer plenty therapeutic opportunities in treating osteoporosis. However, targeting Wnt pathway by using Wnt agonist is impractical because recombinant Wnt is difficult to deliver due to their hydrophobic and insoluble nature. Instead, current approaches targeting Wnt signaling block naturally occurring Wnt antagonists to functionally derepress Wnt signal (Wagner et al., 2011). Two different Wnt antagonists, namely Sclerostin and Dickkopf-1 (DKK-1), are known to inhibit Wnt signaling by interacting with the Wnt coreceptor, LRP5/6. By using antibodies to these proteins, we can expect to reactivate Wnt signals, thus stimulating osteoblasts (Wagner et al., 2011). Considering the direct role of Wnt pathway in stimulating osteoblastogenesis and inhibiting osteoclastogenesis, a pharmaceuticals that can directly promote Wnt signaling may hold promise for fighting osteoporosis.

In various small and large preclinical animal models, NELL-1 has been proven as efficacious in regenerating bone, when locally delivered with surgical implants, as bone morphogenetic protein 2 (BMP-2), the most commonly used osteoinductive growth factor in the market. Considering that a growing number of complications related to the marketed BMP-2 use are being reported (Mroz et al., 2010), a need for a safe but still effective alternative therapeutics is arising. Moreover, previous studies have evidenced that NELL-1 exhibits high specificity to osteochondral lineage cells compared to other growth factors such as BMP. This may be due to its preferential binding to specific receptors on osteochondral lineage cells (Zhang et al., 2010). Importantly, while other growth factors show functional heterogeneity that can lead multipotent MSCs to differentiate into various cell types, NELL-1 exclusively promotes osteochondral lineage cells with high specificity (Zhang et al., 2010). This is an important characteristic when

considering undesirable clinical complications associated with other growth factors such as BMP-2.

Interestingly, a recent genome-wide association study identified several candidate genes related to osteoporosis. By evaluating 433,510 single nuclear polymorphisms in 2,073 women and associating them with multiple osteoporosis related traits, they found that NELL-1 polymorphism is significantly associated with both lumbar spine and femoral neck BMD loss, implicating the association between NELL-1 and osteoporosis (Karasik et al., 2010). In line with this, NELL-1 has exhibited dual anabolic and anti-resorptive properties *in vitro* and *in vivo* in our preliminary studies. Indeed, several lines of evidence indicate potential crosstalk between NELL-1 and Wnt signaling pathway (James et al., 2013). Despite our recent success in reversing ovariectomy-induced bone loss in mice by systemic administration of NELL-1, the frequent dosing (q2d) has questioned the effectiveness of systemic delivery approach. Comparing with other investigational combined anabolic and anti-resorptive drugs such as anti-Wnt antagonists which are mostly designed to inject every 4 day, NELL-1 shows relatively short biological half-life due to the rapid clearance of the native protein.

To overcome this limitation, we sought to find a method to improve pharmacokinetics of NELL-1 protein. Thus, in this study, we investigated if the chemical modification of the NELL-1 protein using polyethylene glycol (PEG) polymers would improve its circulating time while maintaining protein's stability and bioactivity, when intravenously administered with a similar or improved injection schedule than other systemic therapeutics currently in development (anti-DKK-1 or anti-Sclerostin; administered twice weekly). To achieve this, the study was performed

in two folds - *in vitro* thermostability and bioactivity testing, and *in vivo* biological half-life and osteogenic potential experiments.

In the *in vitro* thermostability test, PEGylated NELL-1 demonstrated a higher stability than naked NELL-1. Moreover, we have found in the *in vitro* bioactivity test using mouse calvarial osteoblasts and human perivascular stem cells (hPSCs) that although PEGylation slightly reduces the bioactivity of NELL-1 protein, PEG-NELL-1 still retains significant osteogenic potential compared to the no treatment control. PEG-NELL-1 (5K), in particular, demonstrated a similar bioactivity to that of unmodified NELL-1 as assessed by ALP and ARS staining. In regards to the effect on *in vivo* biological half-life, PEGylation was found to significantly increase the systemic circulation time of NELL-1 from 5.5 hours to 14.5 hours (PEG-NELL-1 (5K); 2.6-fold) up to 31.3 hours (PEG-NELL-1 (20K); 6-fold). Based on the *in vitro* results and *in vivo* half-life assessment, PEG-NELL-1 (5K) was selected as the choice of PEGylated NELL-1 for the following systemic osteogenic potential study, administered at q4d and q7d intervals. PEG-NELL-1 (5K) had (1) the highest thermostability among the three types of PEG-NELL-1 tested, (2) the bioactivity similar to that of unmodified NELL-1, and (3) an enhanced *in vivo* half-life compared to unmodified NELL-1.

Finally, the systemic administration of PEG-NELL-1 over 4-week experimental period significantly improved BMD and percent bone volume (BV/TV) in femurs of 3-month old mice with both q4d and q7d injection schedules. While the q4d and q7d PEG-NELL-1 groups did not show notable differences between each other, the q7d group in particular, showed statistically significant improvement in all measured DXA and microCT parameters compared to PEG/PBS

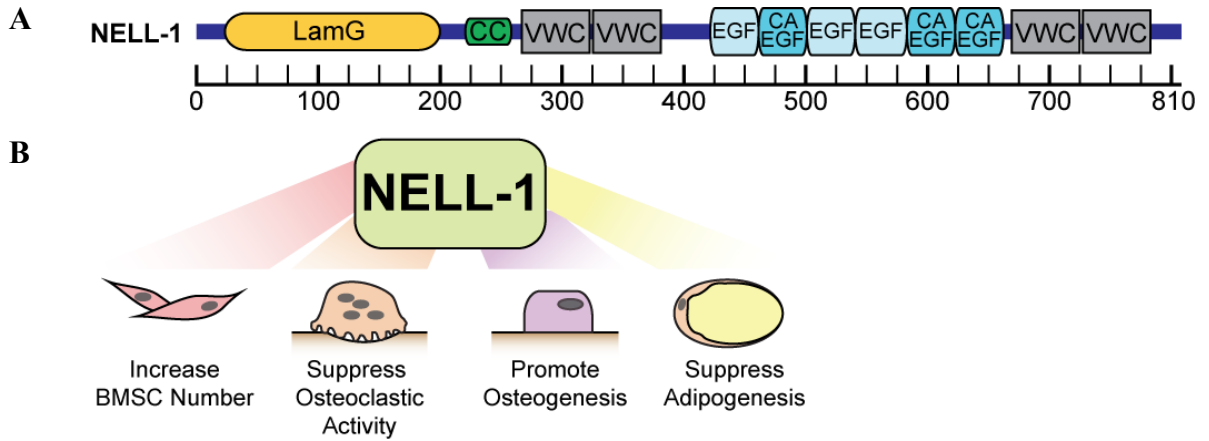
control. These exciting findings encourage us to further investigate the potential of PEGylated NELL-1 as a systemic osteoporosis therapy with an improved injection schedule to ensure better patient compliance in chronic treatment clinical settings.

The presented success in the PEGylation method is innovative and novel in the field of orthopedic research when compared to the conventional controlled-release methods such as lyophilization or absorption onto carriers (e.g. calcium apatite, collagen, or polymers) for surgical implant use. This exciting discovery presents PEGylated NELL-1 as a novel systemic therapeutic agent for the treatment of various osteopenic disorders such as osteoporosis as well as for the healing of large post-surgical orthopedic and craniofacial defects including post-cleft palate or cranial suture repair. Furthermore, current study validates that the PEGylation method is a revolutionary platform technology which prompt us to look into potential application of the method for the effective delivery of other osteogenic growth factors as well.

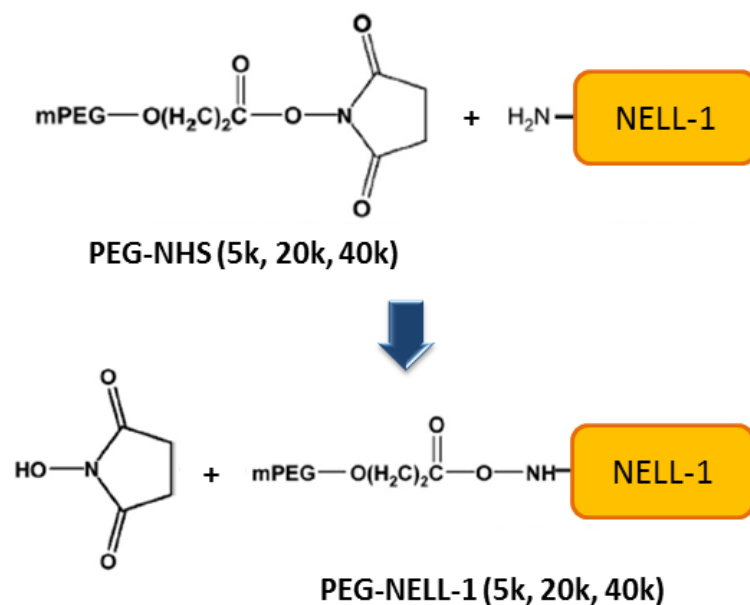
## **CONCLUSION**

In the present study, we demonstrated that PEGylation method successfully improves the thermostability and pharmacokinetics of the NELL-1 protein, while retaining the bioactivity of the protein comparable to that of unmodified NELL-1. Moreover, systemically administered PEGylated NELL-1 demonstrated a considerable osteoinductive potential in healthy mice with reduced dosing schedule (q4d and q7d). The significance and novelty of the present study is that we employed an efficacious approach to develop NELL-1 into a growth factor-based systemic therapy that has a far broader spectrum of application and patient pool than the conventional growth factor-based local therapeutics. Further studies will test the efficacy of systemic PEG-NELL-1 therapy for the reversal of osteoporotic conditions with various murine osteoporosis models such as ovariectomy-induced and extreme disuse atrophy mouse osteoporotic models.

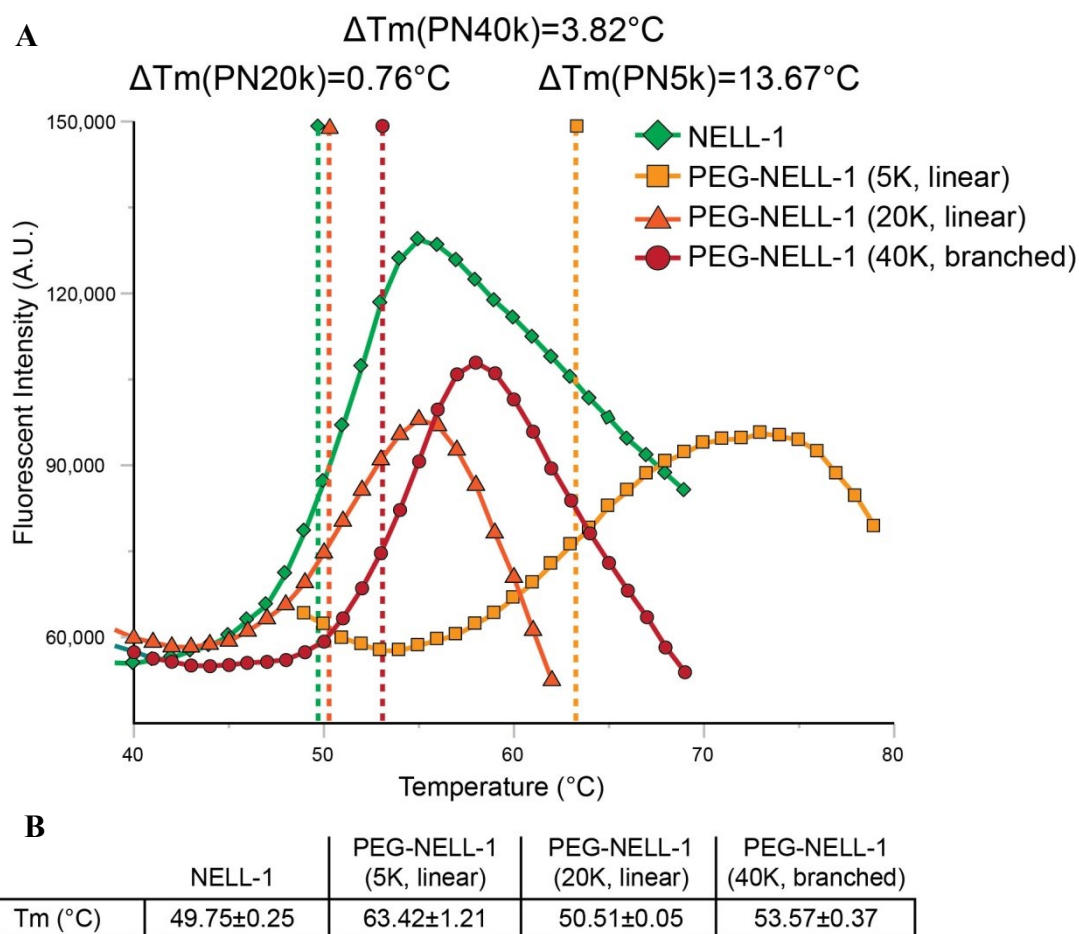
## FIGURES AND TABLES



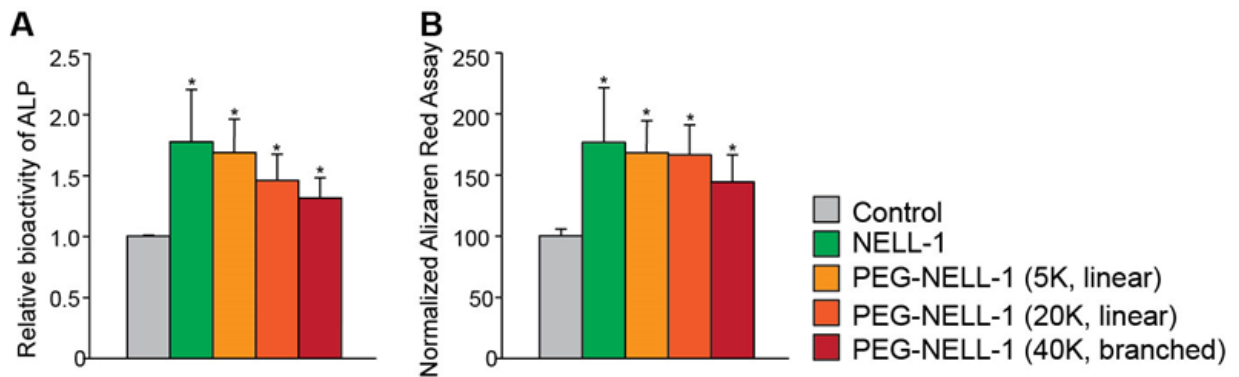
**Figure 1. Structure and function of NELL-1.** (A) Distinct domains within the structure of NELL-1 include LamG: Laminin G domain, VWC: Von Willebrand type C domain, CC: Coiled-coil regions, CA EGF: Calcium binding EGF-like domains. (B) Known functions of NELL-1 to date (James et al., 2013; Zhang et al., 2011b; James et al., 2012; James et al., 2011).



**Figure 2. Schematic diagram of PEG-NELL-1 synthesis.** PEGylation of NELL-1 was achieved by a reaction in which the N-hydroxysuccinimide group of PEG-NHS was covalently linked to the amine group of NELL-1 protein.

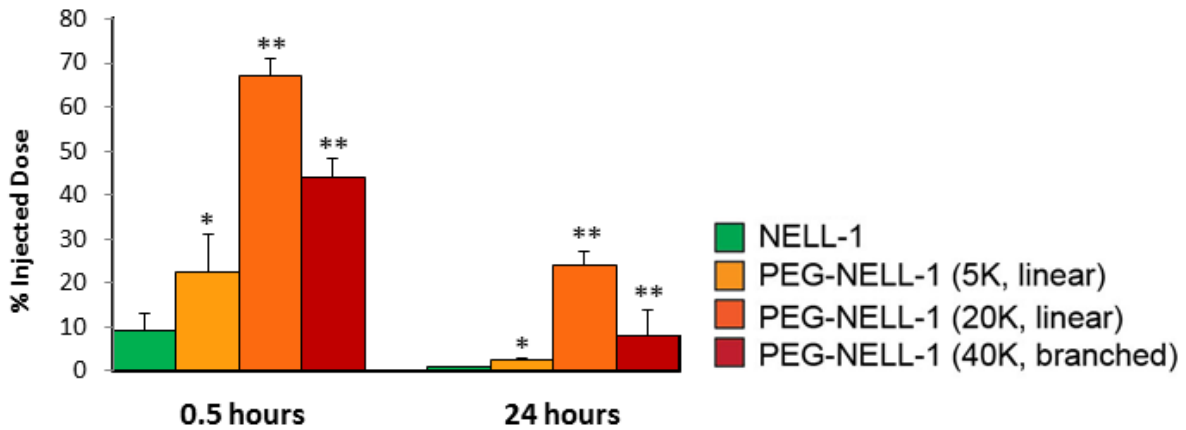


**Figure 3. Thermal shift assay result of NELL-1 and PEG-NELL-1 (5K, 20K, 40K) measured by thermofluor method.** (A) Thermofluor-based protein unfolding curve in PBS buffer. The solid lines represent non-linear fits using Boltzmann model. (B) Comparison of the melting point ( $T_m$ ) and thermal shift amount ( $\Delta T_m = T_m - T_0$ ). The higher  $T_m$  of PEG-NELL-1 compared to NELL-1 suggests that PEGylation enhances the thermostability of NELL-1 protein.

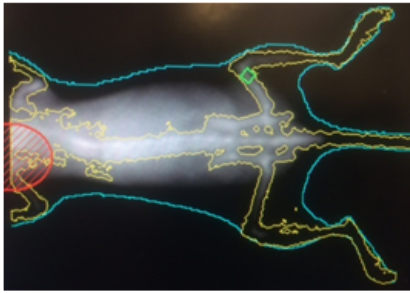
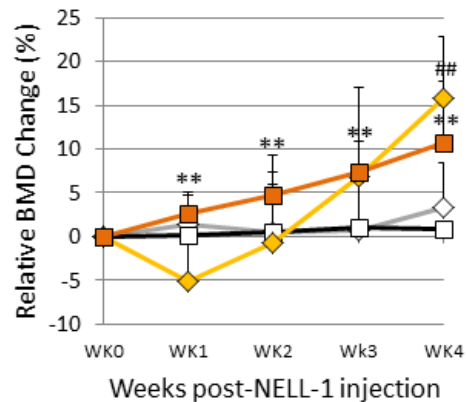
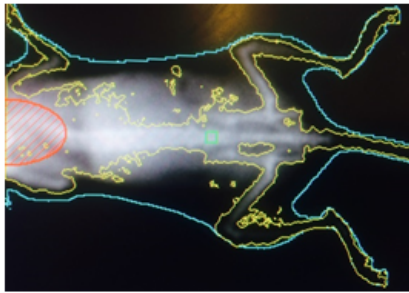
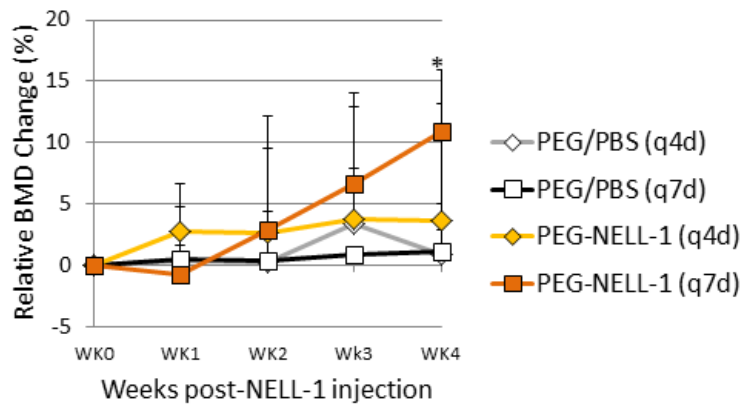


**Figure 4. Effects of PEGylation on pro-osteogenic bioactivity of NELL-1 protein *in vitro*.**

(A) Quantification of ALP expression in mouse calvarial osteoblast cells after 9-day incubation, and (B) quantification of ARS staining in human PSCs after 15-day incubation, treated with NELL-1 or PEG-NELL-1 (5K, 20K, 40K) at a concentration of 300 ng/ml. The results indicate that although PEGylation affects the bioactivity of NELL-1, PEG-NELL-1 still significantly enhances the osteogenic potential of the cells compared to negative control. \* $p < 0.05$ .



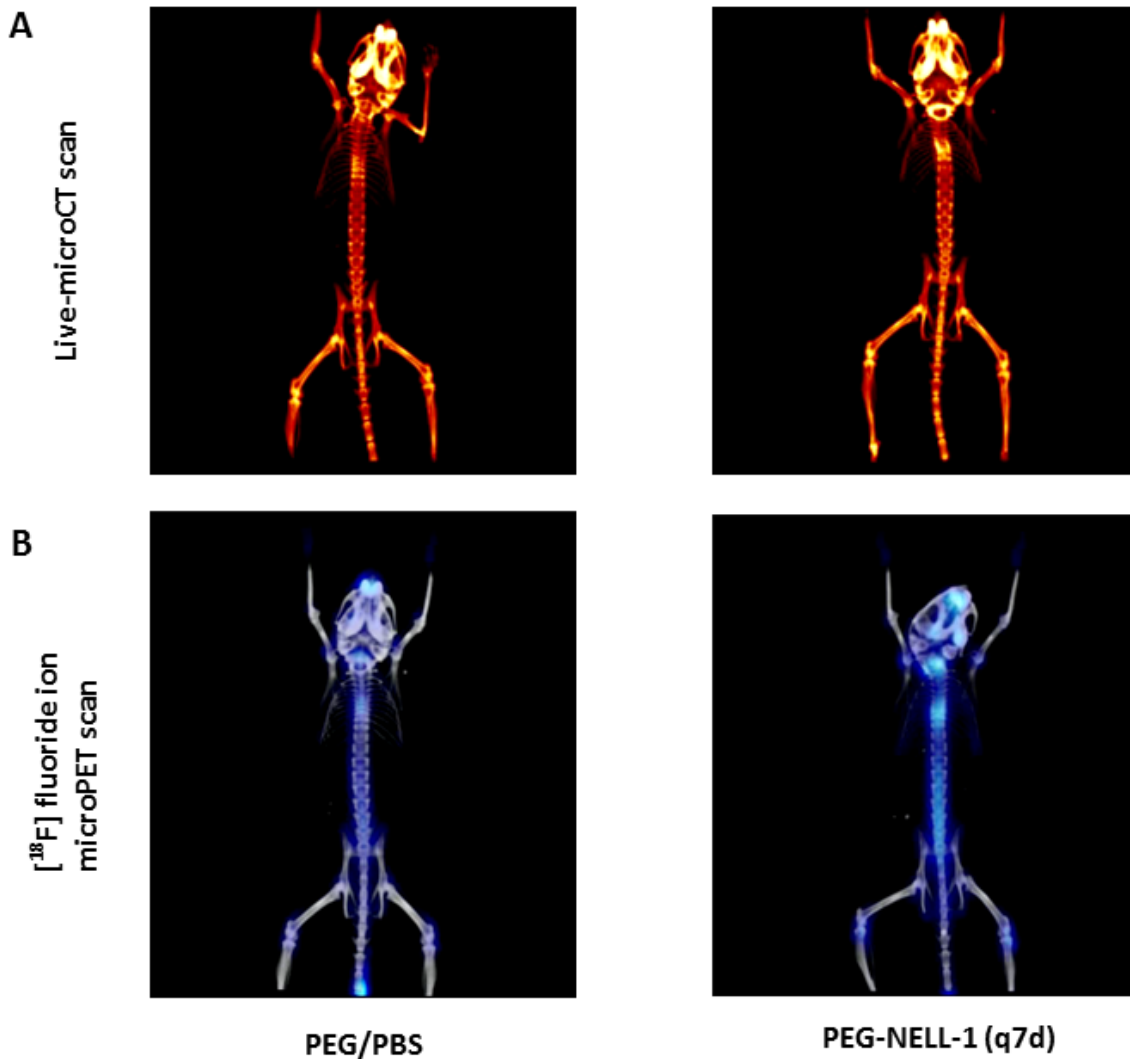
**Figure 5. Effects of PEGylation on biological half-life of NELL-1 protein.** Remaining amount (%) of NELL-1 and PEG-NELL-1 (5K, 20K, 40K) in blood samples after 0.5 hours and 24 hours of injection was measured by the fluorescence intensity of FITC. All three PEG-NELL-1 types demonstrate significantly higher blood concentrations detected at 0.5 and 24 hours compared to that of unmodified NELL-1. \* $p < 0.05$ , \*\* $p < 0.01$ .

**A****Distal Femur****B****Lumbar Vertebrae (L6)**

$$\text{Relative \% BMD Change} = \left( \text{Mean of } \frac{\text{Week X value (DXA X)}}{\text{Week 0 value (DXA 0)}} - 1 \right) \times 100$$

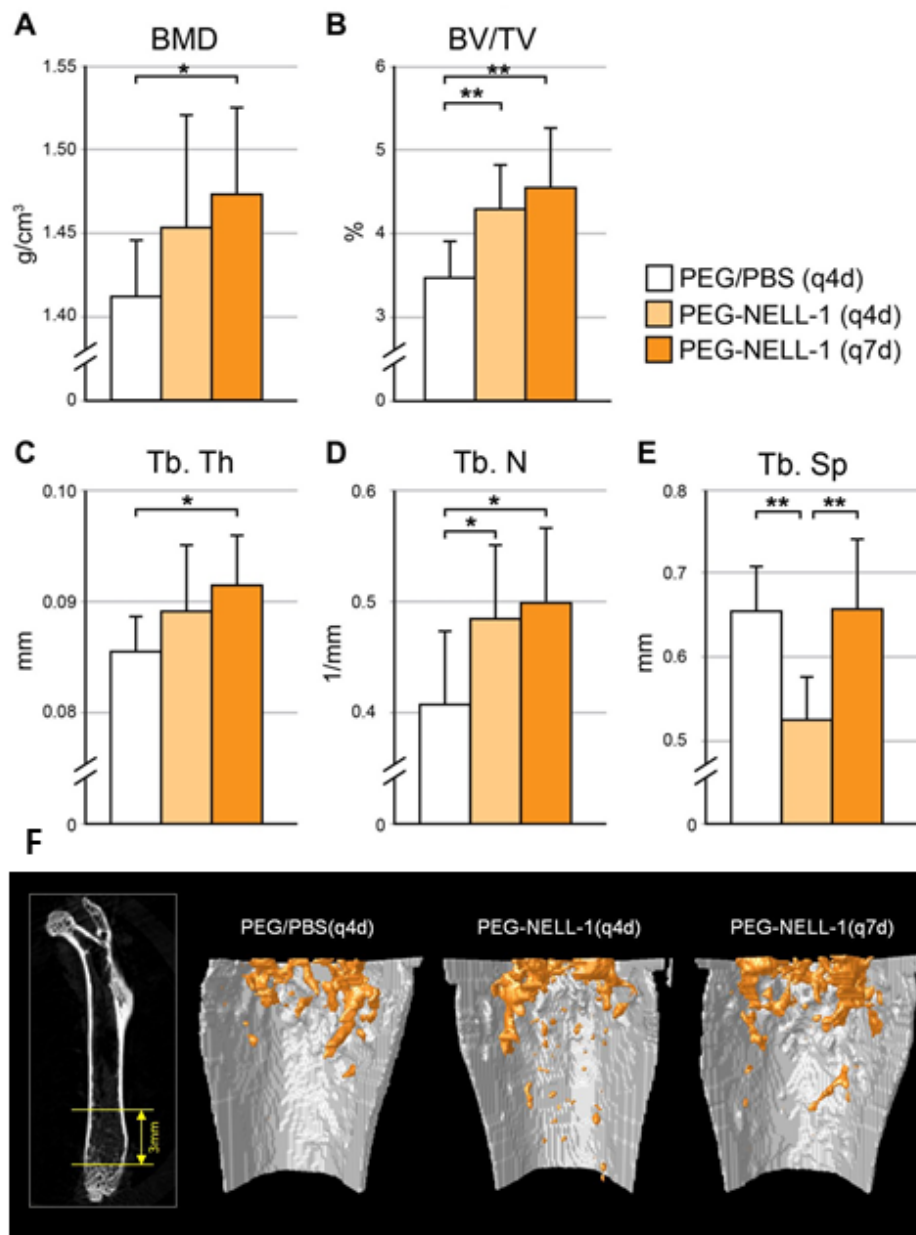
**Figure 6. Dual-energy X-ray absorptiometry (DXA) taken weekly to monitor the changing BMD in femur and lumbar vertebrae.** (A) By 4 weeks post-treatment, q4d and q7d PEG-NELL-1 femurs showed a gradual and significant increase compared to their respective pre-treatment values. Both PEG-NELL-1 groups also demonstrated statistically significant increases in femoral BMD compared to PEG/PBS control, but with no considerable difference between each other. (B) Lumbar vertebrae in both PEG-NELL-1 groups exhibited increasing BMD relative to the baseline throughout the experiment, with more BMD increment observed in q7d

PEG-NELL-1 group than in q4d PEG-NELL-1 group. At week 4, q7d PEG-NELL-1 lumbar vertebrae showed significantly higher BMD increase than that of the vehicle-treated group. No significant difference in lumbar BMD was observed between the two experimental groups at week 4. ##p<0.01 for PEG-NELL-1 (q4d) and \*P<0.05, \*\*p<0.01 for PEG-NELL-1 (q7d), compared to PEG/PBS control.



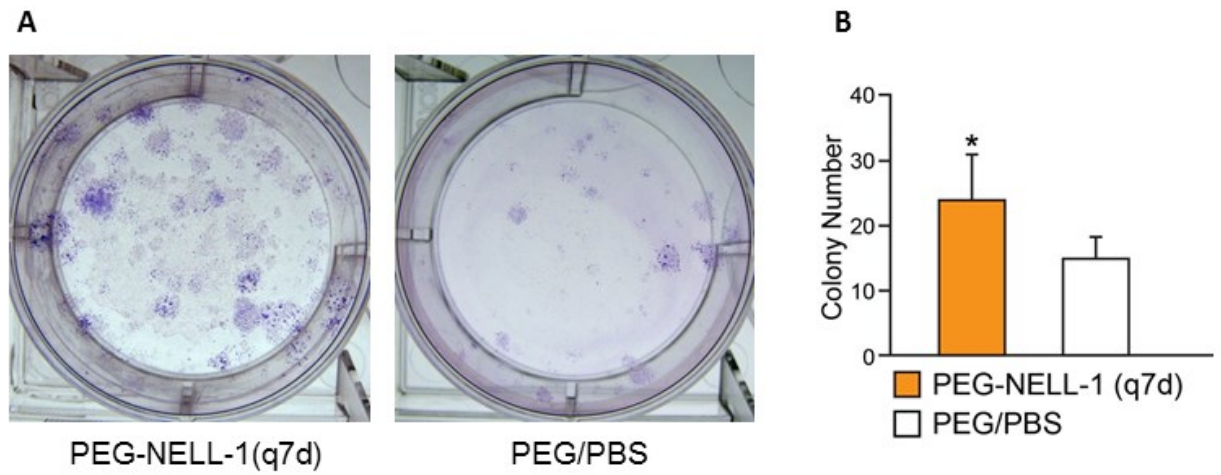
$$\% \text{ ID/cc} = \frac{\text{Tissue activity concentration } (\mu\text{Ci/cc})}{\text{Decay-corrected injected dose } (\mu\text{Ci})} \times 100$$

**Figure 7. MicroPET/CT bone scan using [<sup>18</sup>F] fluoride ion to assess bone turnover rate over the skeleton.** (A) Live-microCT showed increased bone mineral density in PEG-NELL-1 (q7d) group in the overall skeleton. (B) [<sup>18</sup>F] fluoride ion activity distribution demonstrated increased bone turnover rate in PEG-NELL-1 (q7d)-treated mice compared to the control mice, particularly in the vertebral column, proximal humeri, proximal and distal femurs, and proximal tibias.

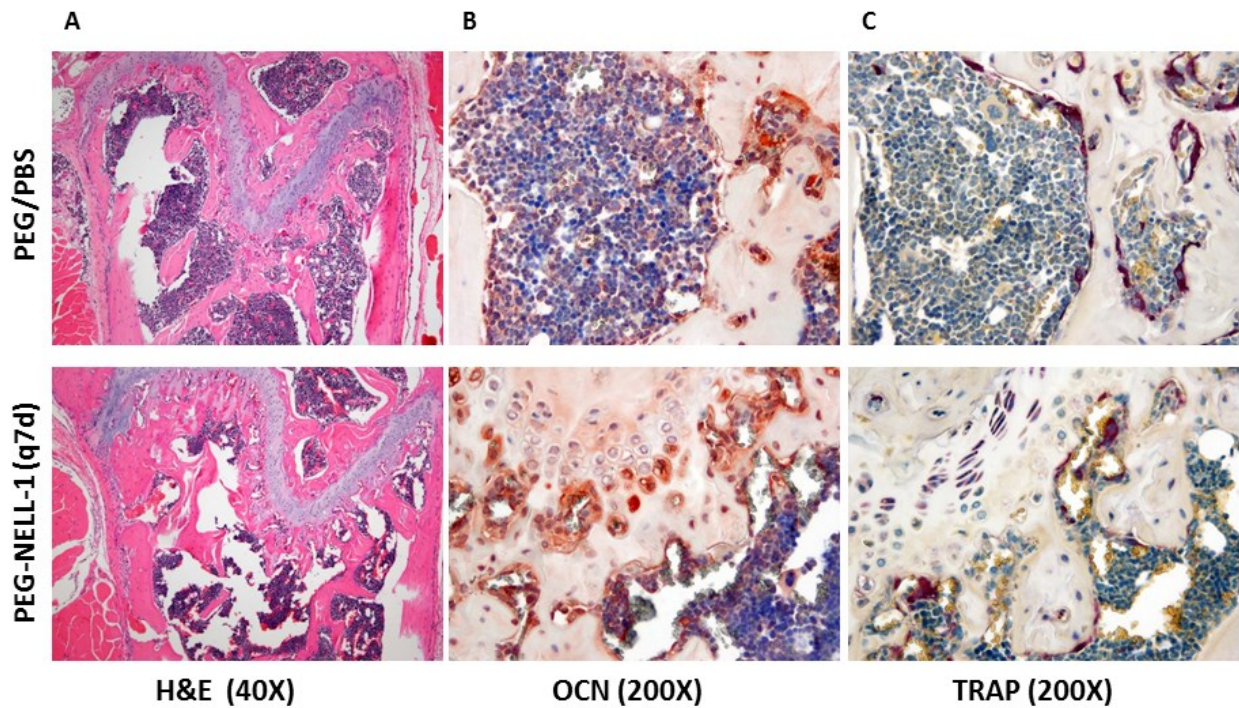


**Figure 8. Post-mortem microCT results at 4 weeks post-treatment.** Both q4d and q7d PEG-NELL-1 group femurs show considerable increases in the trabecular BMD (A), BV/TV (B), and structural parameters including Tb.Th, Tb.N, Tb.Sp (C-E) compared to PEG/PBS control. Both PEG-NELL-1 groups present statistically significant percent bone volume increases compared to

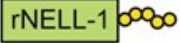
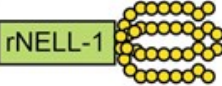
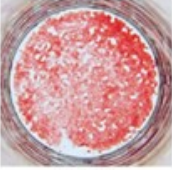
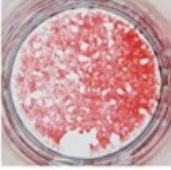
the control (B), but with no significant difference between each other. The q7d PEG-NELL-1 group exhibited significant improvement in all the other trabecular values as well (BMD, Tb.Th, Tb.N, and Tb.Sp) compared to the control (A-E). (F) Region of analysis and 3D reconstruction of representative femur samples. \* $p < 0.05$ , \*\* $p < 0.01$ .



**Figure 9. CFU-F assay results from PEG-NELL-1 (q7d) and PEG/PBS control groups at 4 weeks post-treatment.** (A) CFU-F-derived colonies were stained using Giemsa Staining Solution. (B) Quantification of BMSC content after counting colonies microscopically. PEG-NELL-1 (q7d) group shows significantly increased BMSC content compared to control. \* $p < 0.05$ .



**Figure 10. Histological and immunohistochemical staining results.** (A) H&E staining showed greater trabecular bone formation at the distal femoral metaphysis in the PEG-NELL-1-treated group than control group. (B) Immunostaining also showed more osteocalcin (OCN) positive cells with intense staining in the PEG-NELL-1 group. (C) TRAP staining showed reduced TRAP positive cells in the PEG-NELL-1-treated femurs compared to PEG/PBS control group.

<b>Table 1. PEGylation of rNELL-1</b>				
	rNELL-1	PEG-rNELL-1 (5K)	PEG-rNELL-1 (20K)	PEG-rNELL-1 (40K)
PEG type	---	5,000 Da, Linear	20,000 Da, Linear	40,000 Da, Branched
Schematic structure (PEG-NELL-1 degree)	 0%	 72.6%	 46.9%	 14.2%
Representative Plates & Relative Bioactivity <sup>a</sup>	 100%	 95.5%	 94.3%	 82.0%
$t_{1/2}$ <sup>b</sup>	5.5 hrs	14.5 hrs	31.3 hrs	29.4 hrs

<sup>a</sup> The relative bioactivity of the PEGylated rNELL-1 were determined by quantitative alizarin red-based assay of mineralized primary human adipose-derived stem cells incubated with proteins at a concentration of 300 ng/mL for 15 days.

<sup>b</sup> Elimination half-life was calculated after PEG-rNELL-1 (tagged with FITC) was injected and blood samples were collected at various timepoints (30 min - 48hrs). Concentration of PEG-rNELL-1 was analyzed by monitoring the fluorescence intensity of FITC using a plate reader.

## REFERENCES

- Albers J, Keller J, Baranowsky A, Beil FT, Catala-Lehnen P, Schulze J *et al.* (2013). Canonical Wnt signaling inhibits osteoclastogenesis independent of osteoprotegerin. *J Cell Biol* 200(4):537-549.
- Aghaloo T, Cowan CM, Chou YF, Zhang X, Lee H, Miao S *et al.* (2006). Nell-1-induced bone regeneration in calvarial defects. *The American journal of pathology* 169(3):903-915.
- Aghaloo T, Jiang X, Soo C, Zhang Z, Zhang X, Hu J *et al.* (2007). A study of the role of nell-1 gene modified goat bone marrow stromal cells in promoting new bone formation. *Mol Ther* 15(10):1872-1880.
- Aghaloo T, Cowan CM, Zhang X, Freymiller E, Soo C, Wu B *et al.* (2010). The effect of NELL1 and bone morphogenetic protein-2 on calvarial bone regeneration. *Journal of oral and maxillofacial surgery : official journal of the American Association of Oral and Maxillofacial Surgeons* 68(2):300-308.
- Asatrian G, James AW, Chung C, Velasco O, Zhang X, Ting K *et al.* (2013). Systemic administration of the osteoinductive growth factor NELL-1 promotes bone formation in osteoporotic Mice. *Military Health System Research Symposium (Conference)*.
- Bansal R, Post E, Proost JH, de Jager-Krikken A, Poelstra K, Prakash J (2011). PEGylation improves pharmacokinetic profile, liver uptake and efficacy of Interferon gamma in liver fibrosis. *Journal of controlled release : official journal of the Controlled Release Society* 154(3):233-240.
- Berry SD, Kiel DP, Donaldson MG, Cummings SR, Kanis JA, Johansson H *et al.* (2010). Application of the National Osteoporosis Foundation Guidelines to postmenopausal women and men: the Framingham Osteoporosis Study. *Osteoporosis international : a journal established as result of cooperation between the European Foundation for Osteoporosis and the National Osteoporosis Foundation of the USA* 21(1):53-60.
- Bilezikian JP (2008). Combination anabolic and antiresorptive therapy for osteoporosis: opening the anabolic window. *Current osteoporosis reports* 6(1):24-30.
- Cabrera CV, Alonso MC, Johnston P, Phillips RG, Lawrence PA (1987). Phenocopies induced with antisense RNA identify the wingless gene. *Cell* 50(4):659-663.
- Cowan CM, Zhang X, James AW, Kim TM, Sun N, Wu B *et al.* (2012). NELL-1 increases pre-osteoblast mineralization using both phosphate transporter Pit1 and Pit2. *Biochem Biophys Res Commun* 422(3):351-357.
- Cusano NE, Bilezikian JP (2012). Combination anabolic and antiresorptive therapy for osteoporosis. *Endocrinology and metabolism clinics of North America* 41(3):643-654.

Czerwinski E, Badurski JE, Marcinowska-Suchowierska E, Osieleniec J (2007). Current understanding of osteoporosis according to the position of the World Health Organization (WHO) and International Osteoporosis Foundation. *Ortopedia, traumatologia, rehabilitacja* 9(4):337-356.

Glantschnig H, Scott K, Hampton R, Wei N, McCracken P, Nantermet P *et al.* (2011). A rate-limiting role for Dickkopf-1 in bone formation and the remediation of bone loss in mouse and primate models of postmenopausal osteoporosis by an experimental therapeutic antibody. *The Journal of pharmacology and experimental therapeutics* 338(2):568-578.

Heinemann DF (2000). Osteoporosis. An overview of the National Osteoporosis Foundation clinical practice guide. *Geriatrics* 55(5):31-36; quiz 39.

James AW, Pan A, Chiang M, Zara J, Zhang X, Ting K *et al.* (2011). A new function of Nell-1 protein in repressing adipogenic differentiation. *Biochem Biophys Res Commun.*

James AW, Zara JN, Zhang X, Askarinam A, Goyal R, Chiang M *et al.* (2012). Perivascular stem cells: a prospectively purified mesenchymal stem cell population for bone tissue engineering. *Stem cells translational medicine* 1(6):510-519.

James AW SJ, Velasco O, Asatrian G, Chung G, Khadarian K, Zhang Y, Chang L, Goyal R, Kim J, Zhang X, Adams J, Ting K, Soo C (2013). Systemic administration of NELL-1, a Wnt/ $\beta$ -Catenin Regulator, Induces Bone Formation in Osteoporotic Mice via Integrin $\beta$ 1. American Society of Bone and Mineral Research (ASBMR) Annual Meeting.

Jevsevar S, Kunstelj M, Porekar VG (2010). PEGylation of therapeutic proteins. *Biotechnology journal* 5(1):113-128.

Jilka RL (2003). Biology of the basic multicellular unit and the pathophysiology of osteoporosis. *Medical and pediatric oncology* 41(3):182-185.

Jilka RL (2007). Molecular and cellular mechanisms of the anabolic effect of intermittent PTH. *Bone* 40(6):1434-1446.

Karasik D, Hsu YH, Zhou Y, Cupples LA, Kiel DP, Demissie S (2010). Genome-wide pleiotropy of osteoporosis-related phenotypes: the Framingham Study. *J Bone Miner Res* 25(7):1555-1563.

Kwak J, Zara JN, Chiang M, Ngo R, Shen J, James AW *et al.* (2013). NELL-1 injection maintains long-bone quantity and quality in an ovariectomy-induced osteoporotic senile rat model. *Tissue engineering Part A* 19(3-4):426-436.

Levy Y, Hershfield MS, Fernandez-Mejia C, Polmar SH, Scudiery D, Berger M *et al.* (1988). Adenosine deaminase deficiency with late onset of recurrent infections: response to treatment with polyethylene glycol-modified adenosine deaminase. *The Journal of pediatrics* 113(2):312-317.

- Li W, Lee M, Whang J, Siu RK, Zhang X, Liu C *et al.* (2010). Delivery of lyophilized Nell-1 in a rat spinal fusion model. *Tissue Eng Part A* 16(9):2861-2870.
- Li W, Jara JN, Siu RK, Lee M, Aghaloo T, Zhang X *et al.* (2011). Nell-1 enhances bone regeneration in a rat critical-sized femoral semental defect model. *Plast Reconstr Surg* 127(2):580-587.
- Lu SS, Zhang X, Soo C, Hsu T, Napoli A, Aghaloo T *et al.* (2007). The osteoinductive properties of Nell-1 in a rat spinal fusion model. *Spine J* 7(1):50-60.
- Miner S, Leucht P, Jiang J, Liu B, Zeng A, Fuerer C *et al.* (2010). Wnt proteins promote bone regeneration. *Science translational medicine* 2(29):29ra30.
- Mroz TE, Wang JC, Hashimoto R, Norvell DC (2010). Complications related to osteobiologics use in spine surgery: a systematic review. *Spine (Phila Pa 1976)* 35(9 Suppl):S86-S104.
- Neer RM, Arnaud CD, Zanchetta JR, Prince R, Gaich GA, Reginster JY *et al.* (2001). Effect of parathyroid hormone (1-34) on fractures and bone mineral density in postmenopausal women with osteoporosis. *The New England journal of medicine* 344(19):1434-1441.
- Ng EW, Shima DT, Calias P, Cunningham ET, Jr., Guyer DR, Adamis AP (2006). Pegaptanib, a targeted anti-VEGF aptamer for ocular vascular disease. *Nature reviews Drug discovery* 5(2):123-132.
- Nojima Y, Iguchi K, Suzuki Y, Sato A (2009). The pH-dependent formation of PEGylated bovine lactoferrin by branched polyethylene glycol (PEG)-N-hydroxysuccinimide (NHS) active esters. *Biol Pharm Bull* 32(3):523-526.
- Nusslein-Volhard C, Wieschaus E (1980). Mutations affecting segment number and polarity in *Drosophila*. *Nature* 287(5785):795-801.
- Parfitt AM, Drezner MK, Glorieux FH, Kanis JA, Malluche H, Meunier PJ *et al.* (1987). Bone histomorphometry: standardization of nomenclature, symbols and units. *J Bone Miner Res* 2(6):595-610.
- Shen J, James AW, Zara JN, Asatrian G, Khadarian K, Zhang JB *et al.* (2013). BMP2-induced inflammation can be suppressed by the osteoinductive growth factor NELL-1. *Tissue Eng Part A* 19(21-22):2390-2401.
- Shuler FD, Conjeski J, Kendall D, Salava J (2012). Understanding the burden of osteoporosis and use of the World Health Organization FRAX. *Orthopedics* 35(9):798-805.
- Siu RK, Lu SS, Li W, Whang J, McNeill G, Zhang X *et al.* (2011). Nell-1 protein promotes bone formation in a sheep spinal fusion model. *Tissue Eng Part A* 17(7-8):1123-1135.

Takada I, Kouzmenko AP, Kato S (2009). Wnt and PPARgamma signaling in osteoblastogenesis and adipogenesis. *Nat Rev Rheumatol* 5(8):442-447.

Ting K, Vastardis H, Mulliken JB, Soo C, Tieu A, Do H *et al.* (1999). Human NELL-1 expressed in unilateral coronal synostosis. *J Bone Miner Res* 14(1):80-89.

Vahle JL, Sato M, Long GG, Young JK, Francis PC, Engelhardt JA *et al.* (2002). Skeletal changes in rats given daily subcutaneous injections of recombinant human parathyroid hormone (1-34) for 2 years and relevance to human safety. *Toxicologic pathology* 30(3):312-321.

Wagner ER, Zhu G, Zhang BQ, Luo Q, Shi Q, Huang E *et al.* (2011). The therapeutic potential of the Wnt signaling pathway in bone disorders. *Current molecular pharmacology* 4(1):14-25.

Watts NB, Lewiecki EM, Miller PD, Baim S (2008). National Osteoporosis Foundation 2008 Clinician's Guide to Prevention and Treatment of Osteoporosis and the World Health Organization Fracture Risk Assessment Tool (FRAX): what they mean to the bone densitometrist and bone technologist. *Journal of clinical densitometry : the official journal of the International Society for Clinical Densitometry* 11(4):473-477.

Zhang X, Zara J, Siu RK, Ting K, Soo C (2010). The role of Nell-1, a growth factor associated with craniosynostosis, in promoting bone regeneration. *J Dent Res* 89(9):865-878.

Zhang X, Ting K, Bessette CM, Culiati CT, Sung SJ, Lee H *et al.* (2011a). Nell-1, a key functional mediator of Runx2, partially rescues calvarial defects in Runx2(+/-) mice. *J Bone Miner Res* 26(4):777-791.

Zhang X, Peault B, Chen W, Lee W, Corselli M, James AW *et al.* (2011b). The Nell-1 growth factor stimulates bone formation by purified human perivascular cells. *Tissue Eng Part A* 17(19-20):2497-2509.